Plasmid xxx (xxxx) xxxx

Contents lists available at ScienceDirect

Plasmid

journal homepage: www.elsevier.com/locate/yplas

Quantifying plasmid dynamics using single-cell microfluidics and image bioinformatics

J.C.R. Hernandez-Beltran[a], J. Rodríguez-Beltrán[b], A. San Millán[b], R. Peña-Miller[a,*], A. Fuentes-Hernández[a,*]

[a] Laboratorio de Biología Sintética y de Sistemas, Centro de Ciencias Genómicas, Universidad Nacional Autónoma de México, 62210 Cuernavaca, Mexico
[b] Department of Microbiology, Hospital Universitario Ramon y Cajal (IRYCIS), Madrid, Spain

ARTICLE INFO

Keywords:
Plasmid dynamics
Fluorescence microscopy
Image processing
Microfluidics

ABSTRACT

Multicopy plasmids play an important role in bacterial ecology and evolution by accelerating the rate of adaptation and providing a platform for rapid gene amplification and evolutionary rescue. Despite the relevance of plasmids in bacterial evolutionary dynamics, evaluating the population-level consequences of randomly segregating and replicating plasmids in individual cells remains a challenging problem, both in theory and experimentally. In recent years, technological advances in fluorescence microscopy and microfluidics have allowed studying temporal changes in gene expression by quantifying the fluorescent intensity of individual cells under controlled environmental conditions. In this paper, we will describe the manufacture, experimental setup, and data analysis pipeline of different microfluidic systems that can be used to study plasmid dynamics, both in single-cells and in populations. To illustrate the benefits and limitations of microfluidics to study multicopy plasmid dynamics, we will use an experimental model system consisting on *Escherichia coli* K12 carrying non-conjugative, multicopy plasmids (19 copies per cell, in average) encoding different fluorescent markers and β-lactam resistance genes. First, we will use an image-based flow cytometer to estimate changes in the allele distribution of a heterogeneous population under different selection regimes. Then we will use a mothermachine microfluidic device to obtain time-series of fluorescent intensity of individual cells to argue that plasmid segregation and replication dynamics are inherently stochastic processes. Finally, using a microchemostat, we track thousands of cells in time to reconstruct bacterial lineages and evaluate the allele frequency distributions that emerge in response to a range of selective pressures.

1. Introduction

Plasmids are significant drivers of microbial ecology and evolution by horizontally transmitting beneficial genes and providing recipient cells with access to novel ecological niches (Wiedenbeck and Cohan, 2011). But the contribution of plasmids to bacterial evolutionary dynamics is not reduced to merely acting as vehicles for the horizontal dissemination of genetic information between strains and species. Recent studies have enlisted a series of benefits associated with carrying genes in plasmids, as opposed to encoding them in the chromosome.

The fixation probability of beneficial mutations and the rate of segregational loss are determined by the number of plasmid copies carried by each cell (Stewart and Levin, 1977) and, therefore, copy number control, as well as timing and mode of plasmid segregation, are important factors influencing the population genetics of plasmid-bearing populations (Paulsson, 2002; Rodriguez-Beltran et al., 2019; Ilhan et al., 2019). As a result, the stochastic nature of replication and segregation of multi-copy plasmids has been studied extensively, both in theory (Ishii et al., 1978; Nordström, 1984; Keasling and Palsson, 1989; Paulsson and Ehrenberg, 2001) and in laboratory conditions (Nordström et al., 1984; Novick, 1987; Del Solar and Espinosa, 2000), showing that copy-number control is a noisy process with events randomly distributed in time (Seneta and Tavaré, 1983) and, therefore, intracellular fluctuations in copy numbers can be seen as a stochastic dynamical system (Keasling and Palsson, 1989).

Similarly, plasmid partition is a random process such that, in the absence of plasmid addiction systems (Mochizuki et al., 2006; Baxter and Funnell, 2015), results in an equal chance for each plasmid to be inherited to each daughter cell and, therefore, in a binomial probability of producing a plasmid-free cell upon division. Of course, this is a simplification, as high-copy plasmids can produce dimers through homologous recombination (Summers, 1991) and intracellular spatial

* Corresponding authors.
E-mail addresses: rpm@ccg.unam.mx (R. Peña-Miller), ayarifh@ccg.unam.mx (A. Fuentes-Hernández).

https://doi.org/10.1016/j.plasmid.2020.102517
Received 17 April 2020; Received in revised form 20 May 2020; Accepted 21 May 2020

structure can result in the asymmetric segregation of plasmids upon division (Wang et al., 2016). Also, low-copy plasmids tend to have active partitioning mechanisms that organize plasmids around a centromere-like site to segregate plasmids symmetrically between daughter cells at division (Salje, 2010). In contrast, plasmids that do not encode partition systems decrease the probability of segregational loss by being present in high-copy-numbers.

But carrying multiple plasmid copies not only increases plasmid stability but can also have important consequences in the adaptive dynamics of plasmid-bearing populations, for instance increasing the rate of fixation of beneficial mutations (Galitski et al., 1995) and accelerating the rate of adaptation to deteriorating environmental conditions (San Millan et al., 2016). Furthermore, once a beneficial mutation appears in a plasmid-borne gene, multicopy plasmids can provide a platform for rapid gene amplification (Nicoloff et al., 2019). By increasing gene dosage, bacterial cells have been reported to transiently enhancing the level of resistance to antibiotics (Santos-Lopez et al., 2017), allowing the population to increase in size and, as a result, increasing the probability of appearance of secondary drug-resistant mutations (Sun et al., 2018).

Moreover, multicopy plasmids produce genomic regions of local polyploidy that can generate heterozygous cells where different alleles coexist at a cellular level, a phenomenon also referred to as heteroplasmy (Novick, 1987). As a result, individual cells can increase their genetic diversity and enable populations to circumvent evolutionary trade-offs (Rodriguez-Beltran et al., 2018). It has also been reported that the multicopy plasmids can increase standing genetic variation in the population, thus enabling bacterial populations to escape extinction following a sudden environmental change (Santer and Uecker, 2019). In the absence of selection, however, random genetic drift of multicopy plasmids during cell division (also known as segregational drift (Ilhan et al., 2019)) can reduce the rate of adaptation, despite high-copy plasmids having increased mutational supply.

By focusing on large population sizes, laboratory studies have been able to characterize the interaction between genetic dominance and strength of selection, and correlate these traits with the probability of fixation of mutant alleles and the horizontal transmission of plasmid-borne genes (Rodriguez-Beltran et al., 2019). Other plasmid evolution studies have focused on compensatory adaptation (San Millan et al., 2014; Wein et al., 2019; Hall et al., 2020), horizontal transmission (Lopatkin et al., 2017) and co-evolution between hosts and plasmids (Harrison et al., 2015). Altogether, these results highlight the complex interaction between the intracellular plasmid dynamics and the evolutionary dynamics of bacterial populations.

1.1. Single-cell microfluidics

In the past decades, biology and medicine have been rapidly evolving towards using quantitative tools to study complex biological systems. Interdisciplinary studies use statistical, mathematical, and computational tools, combined with experimental and molecular biology, to understand the behavior of individual cells within a population (Artemova et al., 2015) and to predict their response to environmental change (El Meouche and Dunlop, 2018). The benefit of implementing a *bottom-up* approach is that we can follow the life history of individual cells, instead of averaging large populations and making inferences about cellular processes from population-level observations.

Fluorescence microscopy has been previously used to estimate plasmid copy-numbers (Ng et al., 2010; Løbner-Olesen, 1999), as well as to visualize conjugation (Babić et al., 2008), to study horizontal transmission of plasmids (del Campo et al., 2012) and to explore the range of different plasmid-host associations (Shintani et al., 2014). It has also been used to evaluate in situ conjugation in bacterial plant endosymbionts (Bañuelos-Vazquez et al., 2019) and horizontal gene transfer in microbiomes (Pinilla-Redondo et al., 2018). Moreover, with the use of fluorescent probes, microscopy studies have been able to study with great detail the spatio-temporal distribution of plasmids inside a cell, as well as the segregation dynamics occurring upon division (Wang et al., 2016; Reyes-Lamothe et al., 2013; Hsu and Chang, 2019). These single-molecule studies, however, only consider a small set of cells and are constrained to short-term experiments in constant environments.

On the other hand, microfluidic devices have been used in combination with fluorescence to obtain time-series of gene expression of individual cells (Young et al., 2012; Tomanek et al., 2020). Microfluidic devices can be fabricated using soft lithography (Zhang et al., 2012; Pan et al., 2011), micro-droplets (Boedicker et al., 2009) and protein-based micro-3D printing (Connell et al., 2014). In general, the goal of these devices is to restrict the movement of bacterial cells to observe them for long time intervals with the aim of studying, for instance, gene expression dynamic (Young et al., 2012; Baumgart et al., 2017; Bennett and Hasty, 2009; Locke and Elowitz, 2009), as well as to evaluate the consequences of asymmetric division and cell-to-cell variability of key cellular processes (El Meouche and Dunlop, 2018; Mosheiff et al., 2017; Bergmiller et al., 2017). A brief overview of different microfluidic devices and their uses can be found in (Bennett and Hasty, 2009; Potvin-Trottier et al., 2018).

A myriad of computer vision algorithms have been developed to analyze time-lapse movies acquired using a fluorescent microscope (Young et al., 2012; Van Valen et al., 2016; Berg et al., 2019a; Balomenos et al., 2017; Arnoldini et al., 2014; Sachs et al., 2016; Lugagne et al., 2019; Kamentsky et al., 2011). Of note, *Schnitzcell (Young et al., 2012)* was designed to study colonies of rod-shaped bacteria (e.g. *Escherichia coli* and *Bacillus subtilis*) growing in agar pads, although it is not longer maintained. Recently, novel computational techniques based on machine learning have been successfully incorporated into bio-image analysis pipelines. For example, *DeLTA (Lugagne et al., 2019)* and *DeepCell (Van Valen et al., 2016)* implement deep convolutional neural networks to perform accurate segmentation and lineage reconstruction, while *Ilastik (Berg et al., 2019b)* provides a user-friendly suite for image segmentation and cell tracking.

Besides quantifying single-cell fluorescent intensity, imaging algorithms can also be used to record division events and to estimate duplication and elongation rates of individual bacterial cells. In consequence, microfluidics have been used to study cell growth and homeostasis (Wallden et al., 2016), senescence (Ackermann et al., 2003; Lindner et al., 2008) and bacterial adaptation to stress (Łapińska et al., 2019; Mathis and Ackermann, 2016; Patange et al., 2018). By correlating physiological and morphological properties of individual cells with the level of expression of a gene of interest, previous studies have shown that phenotypic heterogeneity can provide functional benefits for bacterial populations, for instance allowing the implementation of division of labor strategies or increasing survival of the population to fluctuating environmental conditions (Ackermann, 2015). Another benefit of single-cell microfluidics is that it allows us to estimate growth rate differences and survival rates in response to environmental change. Therefore microfluidics has been proposed as a strategy for rapid antimicrobial susceptibility determination (Baltekin et al., 2017; Aroonnual et al., 2017) and to study gene regulatory changes that emerge in response to genetic and environmental perturbations (Rochman et al., 2016; Chait et al., 2017)..

In this paper, we combine microfluidics, fluorescent microscopy, and computer vision algorithms to study the interaction between multicopy plasmids and bacterial fitness in dynamic environments. To achieve this goal, we use a previously characterized experimental system consisting of plasmid-mediated β-lactam resistance evolution in *Escherichia coli (Rodriguez-Beltran et al., 2018)*. The objective of this manuscript is to describe the use of fluorescence and multiple image-based technologies to identify the source of noise in the replication and segregation dynamics of multicopy plasmids, as well as to evaluate the effect of selection imposed by antimicrobial substances on the distribution of plasmids exhibited by single-cells and bacterial

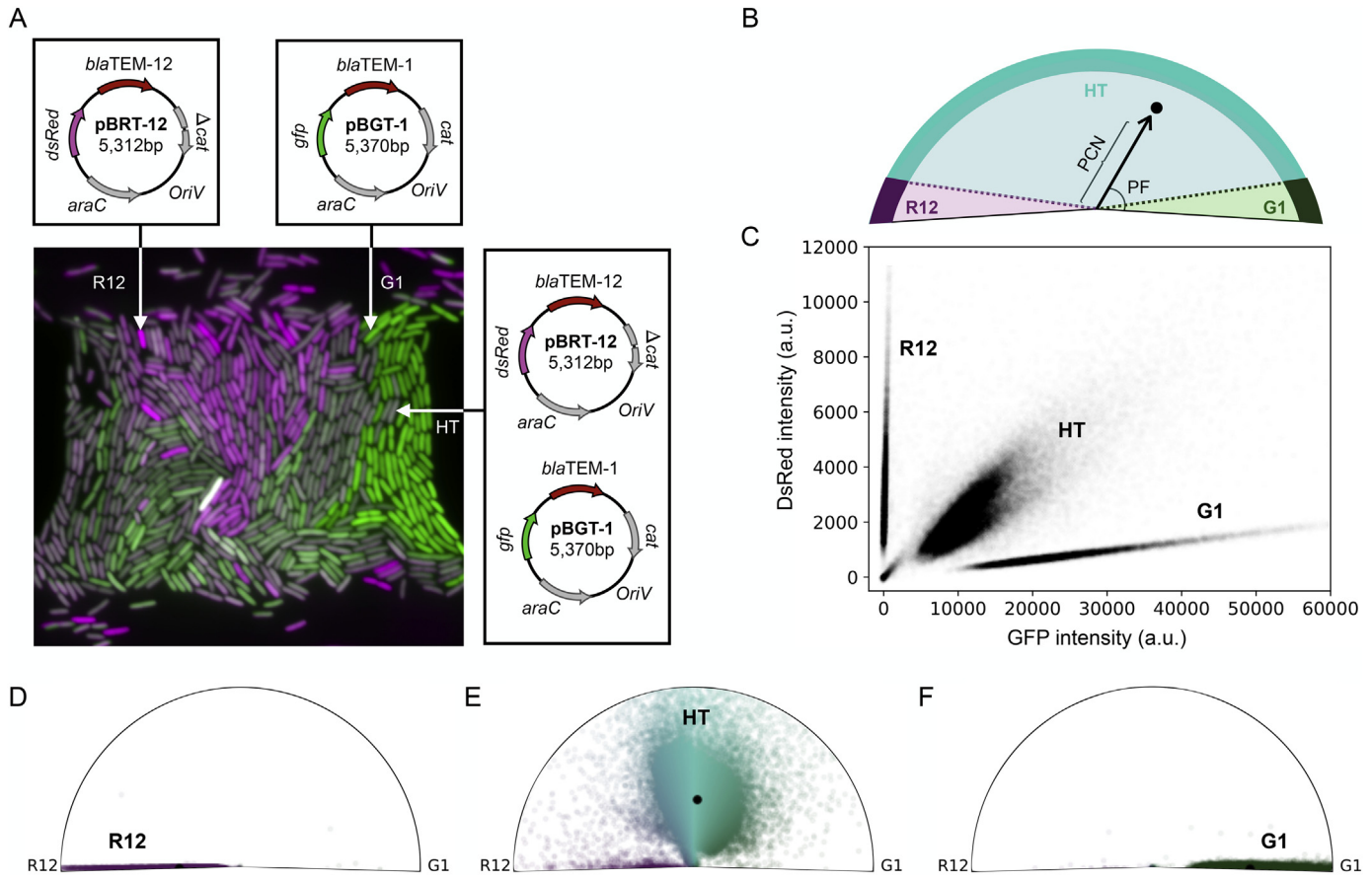

Fig. 1. A) Maps of plasmids used in this study. Composite microscopy image shows a heterogeneous *E. coli* population composed of cells carrying only pBRT-12 (denoted as R12, in magenta), pBGT (G1, in green) and a combination of both plasmids (HT). B) Diagram illustrating a polar representation of multi-channel fluorescent data. After normalizing fluorescence intensities obtained in GFP and DsRed channels, each cell can be represented as a point in a two-dimensional polar coordinate system, where the relative fluorescence between DsRed and GFP channels can be approximated by an angle and the absolute fluorescence intensity from its distance to the origin. We argue that absolute fluorescence is correlated with plasmid copy-number (PCN) and relative fluorescence to the plasmid fraction (PF). C) Raw cytometry data of a heterogeneous population illustrates that a flow cytometer can be used to identify different subpopulations, namely R12, G1 and HT. D-F) Polar representations of different plasmid-bearing populations n drug-free media: D) cells carrying only pBRT-12, E) a heterozygous population where both plasmids co-exist at a cellular level, and F) homozygous cells with only pBGT-1. Black dotes denote the expected value of the corresponding plasmid copy-number distribution. (For interpretation of the references to colour in this figure legend, the reader is referred to the web version of this article.)

populations.

2. Material and methods

2.1. Bacterial strains and plasmids

In this study, we use derivatives of *Escherichia coli* MG1655 strains previously published (San Millan et al., 2016; Rodriguez-Beltran et al., 2018). In short, a β-lactamase gene $bla_{\mathrm{TEM-1}}$ that confers resistance to ampicillin (AMP) was inserted into a small non-transmissible multi-copy plasmid p3655 derived from pSU18T and pBADgfp2, with a ColE1-like (p15a) origin of replication (Le Roux et al., 2007), a plasmid referred to in this study as pBGT-1. This plasmid also contains an eGFP gene under an arabinose promoter with an *araC* repressor. Another plasmid, pBRT, was derived from pBGT by replacing the $bla_{\mathrm{TEM-1}}$ gene with $bla_{\mathrm{TEM-12}}$, a TEM variant that confers resistance to ceftazidime (CAZ) and mild resistance to ampicillin (AMP). Also, eGFP was replaced by a DsRed gene, and the native *cat* resistance gene was knocked-out. In this study, we refer to heterozygous cells simultaneously carrying both plasmids as HT, while G1 and R12 denote homozygous cells bearing pBGT-1 and pBRT-12, respectively (see Fig. 1A for maps of these plasmids). It is important to emphasize that pBGT-1 and pBRT-12 share an origin of replication and only differ in the fluorescent marker and the TEM variant carried. Therefore the plasmid copy-number control mechanism regulates the maximum number of plasmids carried in each cell, independently of the plasmid type.

2.2. Media and growth conditions

Experiments were performed using Lysogeny Broth- Lenox (LB) (Sigma-L3022) supplemented with arabinose (0.5% *w/v*). Antibiotic minimum inhibitory concentrations (MIC) were calculated using standard dose-response curves. To balance HT cells, we prepared the overnight culture using LB media supplemented with 15 mg/l of chloramphenicol and 0.5 mg/l ceftazidime. Stocks solutions at 20% of Arabinose (Sigma-A91906) were prepared by diluting 2 g of arabinose in 10 ml DD water sterilized by filtration. AMP stock solutions (100 mg/ml) were prepared by diluting ampicillin (Sigma-A0166) directly in LB and adding arabinose (0.5%). Stock solutions of ceftazidime (Sigma-A6987) were diluted in water at 10 mg/ml and sterilized by filtering. Chloramphenicol (Sigma-C0378) stock solutions were prepared at 50 mg/ml in ethanol (97%). Population-level experiments were performed using 20 ml of LB media in 125 ml titration flasks. Three replicates of HT cells cultures were grown in balancing media for 24 h in a shaker incubator at 37 °C and 200 rpm.

2.3. Imaging flow cytometry

Population-level experiment measurements were performed by sampling 1 ml of overnight culture and measured their fluorescence using an imaging flow cytometer (Amnis ImageStream Mark II by Luminex). INSPIRE software was used to acquire data discriminating by area, aspect ratio, focus, and side scatter features. GFP fluorescence was excited at 488 nm with 25 mv intensity, and DsRed fluorescence was excited at 561 nm with 200 mv intensity. Populations data files were processed using IDEAS 6.2 software and feature values were exported and analyzed using bespoke scripts implemented in Python programming language.

2.4. Microfluidic devices

We used PDMS (polydimethylsiloxane) microfluidic chips obtained from wafers manufactured using soft photolithography (SU-82000.5, micro resist technology GmbH). In particular, we used a micro-chemostat (Mondragón-Palomino et al., 2011) that contains multiple inputs (a cell-loading input, a shunt, and two for different growth media), as well as two waste outputs. Media inputs are mixed at different proportions using a red fluorescent dye (rhodamine) diluted in one of the media inputs. This device contains 48 chambers of $40x50x.95\ \mu$m, capable of trapping approximately 500 bacterial cells in the same focal plane. Each chamber is open to a big channel on two sides and, when chambers are filled, bacteria in the edges are pushed out of the chamber and washed away. We used this device to obtain high-throughput population-level data derived from single-cell measurements at different time-points. We also used a dual-input mother-machine (Kaiser et al., 2018) device in which bacteria are trapped in a comb-like channels architecture. Mother cells restrained at the bottom of each channel and, as they grow and divide, daughter cells are pushed downwards to a larger channel and washed away. We used this microfluidic chip to keep track of mother cells for very long periods of time, while quantifying fluorescence and other morphological attributes.

2.5. Cell loading and environmental control

Growth media was loaded into 60 ml-syringes connected to the PDMS chip through Tygon tubes and assorted Luer connectors. The pressure inside the chip is controlled with vertical linear actuators and a digital signal generator that controls the height of each syringe. This Dial-A-Wave (DAW) system (Ferry et al., 2011) enables precise control over the extracellular environmental conditions. For the purpose of this paper, we use this DAW to introduce antibiotics into the chip gradually, until reaching a maximum dose that is then maintained until all cells are killed, a protocol we refer to as a ramp experiment. Later we will introduce antibiotics following a sinusoidal signal to alternate selective pressures periodically.

Initial inoculates of HT cells were grown overnight in the presence of sub-lethal doses of chloramphenicol and ceftazidime, in order to clear homozygous cells from the culture and obtain a well-balanced HT culture. A sample was then transferred to 200ml of fresh LB and grown at 30 °C until reaching an $OD_{600} = 0.3$. After centrifuging, cells were re-suspended in 5 ml of LB, and this dense culture was used to inoculate the microfluidic chip. For all microfluidics experiments, we used LB media supplemented with arabinose at 0.5% and Tween20 (Sigma-P2287) at 0.075%. In all cases, cells were allowed to grow and divide multiple cell cycles in a drug-free environment, allowing us to determine the baseline fluorescent intensity of the population. We later use this value to normalize our data and compare fluorescent intensities obtained for different channels.

2.6. Microscopy and image acquisition

Time-lapse images of microfluidic experiments were acquired using a Nikon Eclipse Ti-E epifluorescence microscope equipped with differential interface contrast (DIC), a motorized stage and a perfect focus system that allows us to obtain long-time time-lapses. The microscope was controlled by the Nikon NIS-Elements AR 4.20 program and is equiped with a Lexan Enclosure Unit with Oko-touch temperature control that allows us to incubate the microfluidic chips. The experiments are conducted at 30 °C. For all experiments, time-lapse movies were acquired with a 100× Plan APO objective without analog gain and with field and aperture diaphragms as closed as possible to avoid photobleaching. DIC images were taken at 9v DIA-lamp intensity with exposure of 200 ms, DsRed channel (excitation from 540 to 580 nm, emission from 600 to 660 nm filter) with exposure of 600 ms, GFP channel (excitation from 455 to 485 nm, emission from 500 to 545 nm) with 300 ms exposure. Images were taken every 5 or 10 min, depending on the experiment.

2.7. Image processing and analysis

Microscopy time-lapse movies were analyzed using a semi-automated ImageJ (Schneider et al., 2012) analysis pipeline that implements a deep-learning algorithm for image segmentation (Van Valen et al., 2016). Cell tracking and lineage reconstruction were performed in Python using standard numerical and geometric libraries (NumPy, Shapely, Pandas, Scipy, Matplotlib). Data and code are openly distributed and available for download at https://github.com/ccg-esb-lab/uJ.

In short, the image processing pipeline consists on 1) organizing TIF files generated by NIS Elements, 2) aligning traps and using rigid motion transformation to correct for x-y drift in time-lapse images, 3) using *Parallel Interactive Deconvolution* with a theoretical point spread function generated with PSF Generator to produce a segmentable image, 4) using *DeepCell* (Van Valen et al., *2016*) to segment images and obtain binary masks, 5) cell detection and automatic correction of ROIs, 6) manual correction of a binary mask, 7) data acquisition by overlapping masks in different fluorescent and bright field channels, 9) cell tracking using a feature-aided nearest-neighbor algorithm and lineage reconstruction and, finally, 10) data analysis and visualization. The goal of this image bioinformatics pipeline is to acquire time-series of fluorescent intensity and other morphological properties of individual cells, as well as to obtain population-level statistics to estimate, for instance, the mean cell duplication rate of the population or changes in the shape of the fluorescence distribution.

2.8. Estimation of plasmid copy-number and plasmid frequency

There are two quantities we estimate from fluorescent data: plasmid copy-number (PCN) and plasmid frequency (PF). Previous studies have established that gene copy-number and fluorescent intensity are positively correlated, both when carried in chromosomes (Bergmiller et al., 2017) or in plasmids (Rodriguez-Beltran et al., 2018; Ghozzi et al., 2010). Therefore we will use flow cytometry and fluorescent microscopy to determine the relative intensity of individual cells with respect to the population-level mean (it was previously determined that the plasmids used in this study are carried, on average, ~19 copies of the plasmid per cell) (San Millan et al., 2016).

Also, we estimate the proportion of each plasmid type carried in each cell from the relative fluorescent intensity measured on different channels. Let us define Φ_g and Φ_r the fluorescent intensity of cell i measured in the green and red channels, respectively. As fluorescent proteins have different maturation times and intrinsic brightness (Balleza et al., 2018), we normalized the data by dividing every channel measurements by the maximum intensity and obtained relative intensity values for each channel, quantities that we will denote as $\widehat{\Phi}_g$ and $\widehat{\Phi}_r$.

We argue that, in this case, a polar representation of fluorescent

data is more appropriate, as illustrated in the diagram shown in Fig. 1B. That is, to estimate plasmid fraction from flow cytometry or microfluidic data we will transform the $\hat{\Phi}_g/\hat{\Phi}_r$ ratio into polar coordinates:

$$PF{\sim}\theta := \arctan(\hat{\Phi}_r/\hat{\Phi}_g).$$

This expression allows us to estimate the fraction of plasmids (PF), pBGT-1 plasmid with respect to the pBRT-12 plasmid, a quantity we refer to as *relative fluorescent intensity* and denote as θ. Similarly, we can use r to approximate the absolute plasmid copy number (PCN) by assuming that fluorescent intensity is proportional to the number of copies of the gene carried by each cell,

$$PCN{\sim}r := \sqrt{\hat{\Phi}_g^2 + \hat{\Phi}_r^2}.$$

However, the assumption of a linear relationship between PCN and absolute fluorescent intensity does not always hold and, as discussed extensively in (Tal and Paulsson, 2012), prevents from using absolute fluorescent intensities as a proxy for plasmid copy number. For this reason, in this paper we will restrict our analysis to using θ to evaluate changes in the relative abundances of each allele (i.e. the plasmid fraction) in response to different environmental conditions.

3. Results

3.1. Using flow cytometry to study population dynamics of heterogeneous populations

A fundamental problem in plasmid biology is to determine environmental conditions that enable costly plasmids to be stably maintained in bacterial populations (Harrison et al., 2015; Loftie-Eaton et al., 2016; Porse et al., 2016), This problem is of particular interest for bioengineers and synthetic biologists, as genetic manipulations of microorganisms generally use plasmids as cloning vectors, despite being metabolically costly and, therefore, susceptible to be lost through purifying selection. In contrast, as drug-resistant genes tend to be carried in plasmids (Alekshun and Levy, 2007; San Millan, 2018), it is also a problem of interest for biomedical scientists to determine conditions that cure drug-resistant plasmids of pathogenic populations (Boucher et al., 2009) and to evaluate the probability of fixation of drug-resistance mutations (Ilhan et al., 2019; Rodriguez-Beltran et al., 2018).

Independently of the motivation, experimental studies routinely estimate the fraction of plasmid-bearing cells within a bacterial population by replicating bacterial colonies from non-selective agar plates onto plasmid-selective and non-selective media. In recent years, other studies have used a combination of flow cytometry (FCM) and real-time quantitative PCR (qPCR) to estimate the mean plasmid copy number of the population (Ng et al., 2010) and to determine the relative abundance of plasmid-bearing cells (Bahl et al., 2004). The benefit of the FCM and qPCR is that both are cultivation-independent and provide precise estimations about the mean plasmid copy number of the population.

Here we use an image-based FCM (see Methods) to study the resulting PCN distribution that emerges from exposing genetically-diverse populations to different selection regimes. We focus on a well-characterized experimental system of drug resistance evolution: plasmid-mediated TEM-1 evolution towards ceftazidime resistance in *Escherichia coli*. The numerous ways in which TEM has evolved suggests that it can respond very specifically to each β-lactam, and therefore has been used extensively to study the molecular evolution in response to different selection regimes, both when TEM is encoded in the chromosome (Barlow and Hall, 2002; Barlow and Hall, 2003) or in plasmids (Santos-Lopez et al., 2017; Rodriguez-Beltran et al., 2018). Indeed, nearly every β-lactamase that has been identified as a resistance determinant among clinical bacteria has experienced molecular evolution in response to the use of different β-lactam antibiotics, with over 215 variant TEM β-lactamases identified with differences in amino acid sequence and susceptibility to β-lactam antibiotics (Barlow and Hall, 2002).

3.1.1. Relative allele frequencies are modulated by selection and segregational drift

Our experimental systems consists of a bacterial population containing small (5.3Kb), non-conjugative, multicopy plasmids (pBGT-1 with mean PCN = 19.12 ± 1.56, and pBRT-12 with 21.1 ± 0.85 plasmids in average (San Millan et al., 2016)), different fluorescent markers (GFP and DsRed respectively, both under the *araC* promoter) and TEM genes that produce different variants of β-lactamase, an enzyme that hydrolyzes the active portion of β-lactam antibiotics (Knox, 1995).

It has been established there is a fitness cost associated with synthesizing fluorophores, in this case, expressed in terms of a reduced growth rate in the presence of arabinose with respect to the same strain growing in arabinose-free environments (two-tailed t-test, p-value < 0.05, $N = 4$). For this reason, all experiments described in this study were performed in the presence of arabinose. Crucially, both fluorescent proteins impose a similar fitness burden and therefore no significant differences in growth rate were observed in populations producing either GFP or DsRed proteins (two-tailed t-test, p-value = 0.512, $N = 6$) (San Millan et al., 2014), therefore allowing us to associate changes in fluorescent intensity to differences in fitness of the corresponding TEM alleles, and not due to differential cost of producing fluorescent proteins.

Fig. 1A displays a composite microscopy image showing that a population of HT cells presents high levels of heterogeneity; while some cells are only detected in DsRed or GFP channels (corresponding to cells with high proportions of either plasmid), other cells exhibit analogous levels of fluorescence in both channels (corresponding to heterozygous cells bearing both pBGT-1 and pBRT-12, mean PCN = 22.3 ± 4.7). Fig. 1C shows raw fluorescent intensity determined with flow cytometry of cells in a heterozygous population, revealing the existence of three main clusters, corresponding to homozygous cells (R12 and G1) and the heterozygous population (HT). All flow cytometry experiments were performed in triplicate, with fluorescence distributions obtained by sampling 20,000 cells from the corresponding population.

Fig. 1D and F show that clonal populations of G1 and R12 are only present in the corresponding region of the polar coordinate system when measured after 24 h of growth. In contrast, HT cells carry both plasmids and are therefore scattered throughout the polar plane. This large dispersion in PCN and PF has been predicted by theoretical models of multicopy plasmid dynamics (Peña-Miller et al., 2015; Münch et al., 2019), suggesting that populations bearing multicopy plasmids can present cell-to-cell differences in total plasmid copy-number and in plasmid frequency. Indeed, recent clinical studies have suggested that gene amplification and copy-number variability in drug-resistance genes yield heteroresistant populations (Andersson et al., 2019), potentially leading to treatment failure in clinical settings (Nicoloff et al., 2019; Wang et al., 2014; Band and Weiss, 2019).

A consequence of bearing plasmids with different variants of TEM is that heterozygous populations exhibit heterogeneous profiles of resistance. In this case, $bla_{\mathrm{TEM-1}}$ provides resistance to ampicillin (AMP), while $bla_{\mathrm{TEM-12}}$ to ceftazidime (CAZ) and partially to AMP (Rodriguez-Beltran et al., 2018; Mroczkowska and Barlow, 2008). So, to determine how different environments modulate the distribution of plasmids, we inoculated a population of HT cells in drug-free media and, after 24 h, used a flow cytometer to obtain the distribution illustrated in Fig. 1E. Similarly, we exposed a heterozygous population to a sub-lethal concentration of ampicillin (8 *mg/ml*) and estimated the resulting plasmid distribution after 24 h (see Fig. 2A). We then repeated this assay with ceftazidime (8 *μg/ml*) and, analogous to AMP, HT cells exhibited large dispersion, while R12 and G1 showed variability in PCN, but not in PF.

We then clustered the population based on their relative fluorescent intensities and counted the number of cells in each group. The relative abundances of each subpopulation are illustrated in Fig. 2E. Note how,

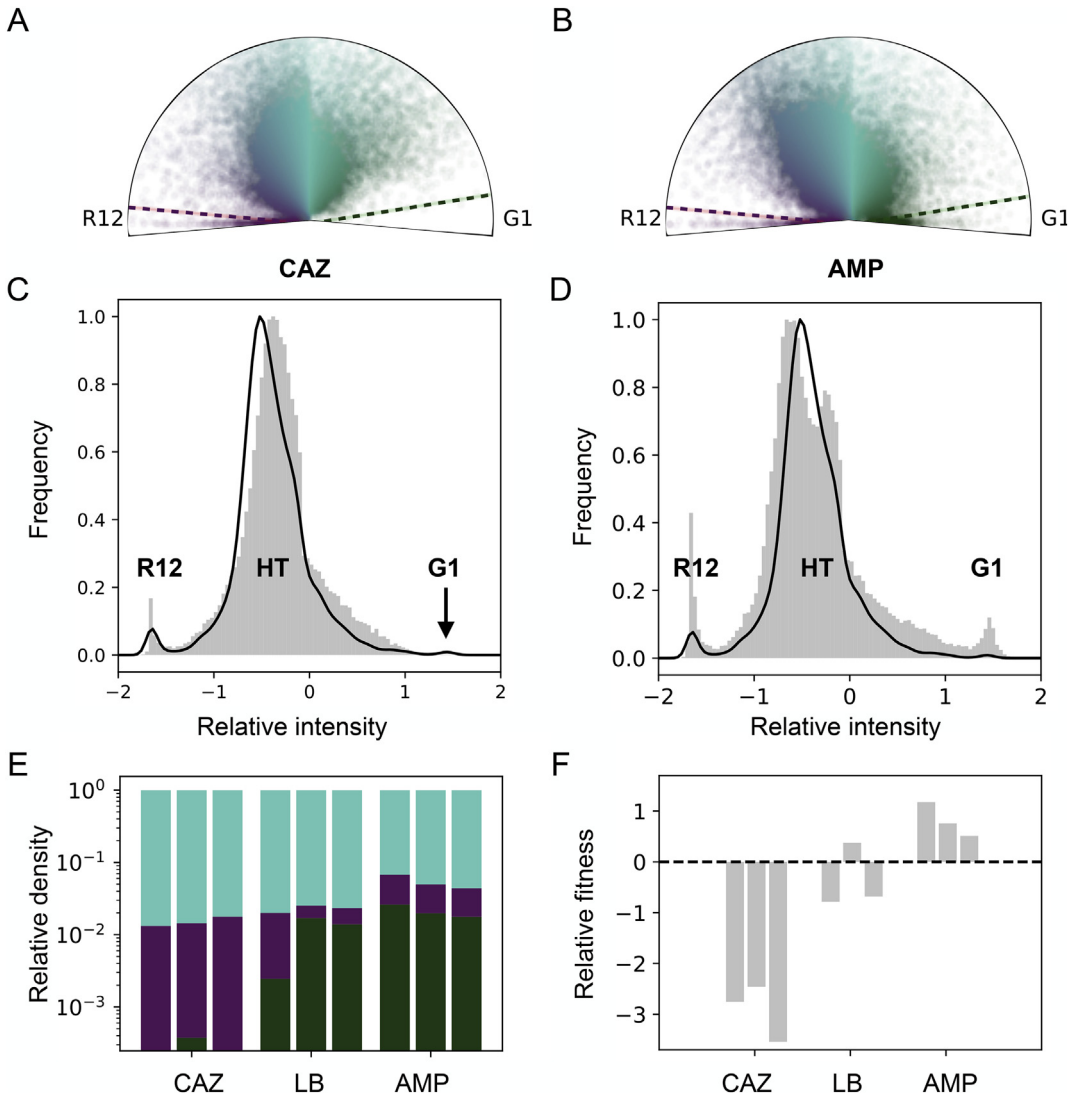

Fig. 2. Polar representation of fluorescent intensities obtained using flow cytometry of HT populations exposed to A) ceftazidime, and B) ampicillin. Distributions were obtained by sampling 60,000 cells from three independent biological replicates. C-D) Histograms of relative intensity for both selection regimes, CAZ and AMP, respectively. Note how AMP maintains a subpopulation of G1 cells, while in CAZ, only HT and R12 cells are present at the end of the experiment (the arrow in C points towards relative intensity values that correspond to G1). This is a consequence of R12 cells being resistant to both antibiotics and G1 only resistant to AMP. In drug-free media, both homozygous populations are present, resulting from the segregation of HT cells into G1 or R12. E) The relative density of each subpopulation under different environmental conditions, determined by clustering cells according to their relative fluorescent intensity. Each bar corresponds to a replicate experiment in each environment ($N = 3$). F) Relative fitness of G1 with respect to R12, after 24 h of growing under different environmental conditions (N = 3). As expected, AMP provides a fitness benefit for G1, while CAZ positively selects for R12.

in drug-free media, segregational instability produces homozygous subpopulations, either carrying $bla_{\mathrm{TEM-1}}$ or $bla_{\mathrm{TEM-12}}$. As $bla_{\mathrm{TEM-1}}$ is susceptible to ceftazidime, we did not observe any G1 cells when HT was exposed to CAZ (left bar in Fig. 2E). The absence of cells with relative fluorescent intensity values in the range corresponding to G1 cells can also be seen in Fig. 2A and C (arrow in 2C shows the location of the G1 subpopulation). In contrast, as $bla_{\mathrm{TEM-12}}$ confers resistance to CAZ, then R12 increased in abundance relative to G1 when exposed to ceftazidime.

Similarly, in environments that positively select for cells carrying plasmids encoding $bla_{\mathrm{TEM-1}}$, the resulting distribution shows an increase in the relative abundance of G1 (right bars in Fig. 2E). Note that, in this case, R12 cells were able to survive treatment with ampicillin, a consequence of a previously reported cross-resistance to both AMP and CAZ provided by the $bla_{\mathrm{TEM-12}}$ gene (Rodriguez-Beltran et al., 2018; Salverda et al., 2010). We also performed statistical tests to analyze the PF distributions of the populations under each selective regime and found that they are significantly different (Kruskal-Wallis H statistic = 649.6, p-value < 0.001). Similarly, pair-wise Kolmogorov-Smirnov tests demonstrated significant differences when performing direct comparisons between AMP-CAZ, AMP-LB, and CAZ-LB distributions (p-values < 0.001).

Based on the relative abundances of each strain, we estimated the relative fitness of G1 with respect to R12 under different selection regimes. Fig. 2F shows that using ampicillin increases the relative frequency of G1 and, as a result, produces an increase in the relative fitness of G1 compared to R12. Conversely, CAZ positively selects for R12, and therefore G1 was suppressed in the population.

Altogether, by analyzing the distribution of fluorescent intensities in different environments, we conclude that selection imposed by antibiotics modifies the relative frequency of different alleles in the population. There are, however, two possible explanations for this behavior: selection acting on populations (this would mean that population-level dynamics is a consequence of changes in the relative abundances of

different subpopulations) or at a level of single-cells (implying that segregation and replication may not be completely stochastic). Using a flow cytometer does not help us differentiate between these possibilities, so, in the remainder of this paper, we will use microfluidic devices that allow us to correlate selection with changes in allele frequency, both at a level of single-cells and in bacterial populations.

3.2. Using microfluidics to analyze plasmid dynamics of individual cells

We have shown that flow cytometry can be used to evaluate the effect of selection in the frequency of heterozygous cells in the population. However, flow cytometry data does not provide time-resolved information about the rate of fixation of different alleles or about the stochastic nature of segregation and replication of plasmids. To overcome these limitations, we used microfluidics to perform long-term observations of individual cells and, with the aid of fluorescent microscopy and image processing algorithms, quantified segregational drift in heterozygous populations.

In particular, we will use a microfluidic device known as a dual-input mother-machine, designed to precisely control the environmental conditions while trapping individual cells in narrow channels under controlled environmental conditions. As cells grow and divide, daughter bacterial cells are pushed downwards to the channel opening and washed away of the device. We will use this microfluidic chip to perform long-term observations of single-cells and quantify temporal changes in the fraction of pBRT-12 and pBGT-1 plasmid, with the aim of studying segregational drift resulting from the stochastic segregation and replication of multi-copy plasmids.

3.2.1. Intracellular plasmid dynamics is stochastic and not influenced by antibiotic selection

The benefit of mother-machine microfluidic devices is that they allow us to culture individual cells for hundreds of generations under the microscope, in contrast to microscope culture protocols which do not actively remove progeny during growth and therefore get rapidly saturated. Multiple mother-machine devices have been proposed (Taheri-Araghi and Jun, 2015; Long et al., 2013), but we will we use a dual-input mother machine (Kaiser et al., 2018), as it allows us to precisely control the concentration of antibiotic inside the microfluidic chip.

First, we performed a long-term experiment consistent on introducing HT cells into the device and observing them for a period of 72 h. We observed four device positions with ~13 microchannels per field of view, leading to 244,249 single-cell measurements, with mean fluorescent intensities of 212 ± 81 for GFP and 155 ± 51 in DsRed, normalized relative intensity of 1.42 ± 0.53, and normalized absolute intensity of 0.46 ± 0.14. By acquiring images in multiple channels (GFP represented in green and DsRed in magenta) we can follow changes in fluorescence intensity between division events. Fig. 3A shows a montage of mother cells at specific time-points, with their corresponding time-series represented in Fig. 3B (black line corresponding to the cell illustrated in Fig. 3A, while grey lines show the relative intensity time-series obtained for other representative cells in the device).

It is important to highlight that time-series shown in Fig. 3B are very long time-series (72 h, up to 99 cell cycles), allowing us to quantify the difference in relative fluorescent exhibited by each cell at the moment of division and to estimate the difference in fluorescence between consecutive cell cycles, a quantity we refer to as Δ *relative intensity*. Fig. 3E shows how the time-series of Δ relative intensity produces increases in one fluorescent channel as frequently as increases in the other direction. As a result, the difference between relative intensity values estimated in consecutive time-points is approximated by a Normal distribution with $\mu = 0.00057$ a $\sigma^2 = 0.0092$ (see Fig. 3D).

Fig. 3F shows the partial autocorrelation function obtained for time-series of relative intensity in a drug-free environment. Note lags > 0 are within the 95% confidence interval, suggesting that changes in plasmid frequency are generated by an auto regressive process of first order, consistent with the tenet that random segregation and replication of plasmids are inherently stochastic processes. Another interesting feature of our data is that intracellular plasmid diversity can be maintained for many generations in individual bacterial cells. Of course, phenotypic delay (Sun et al., 2018) and fluorescent protein stability (Balleza et al., 2018) could also stabilize fluorescence, but only for a few cell cycles.

However, a consequence of the random segregation of plasmids is that there is a probability larger than zero of segregating plasmids unevenly between mother and daughter cells. In our experimental system, this would be reflected as large jumps in Δ relative intensity. Fig. 3C shows a kymograph obtained from a time-lapse movie (Supplementary Movie S1), whereby the cell in the top of the channel (marked with a black triangle) corresponds to the time-series shown in Fig. 3B. Top and middle images correspond to GFP and DsRed channels, while the bottom image illustrates masks obtained after image segmentation, colour-coded to represent the relative intensity value obtained after normalizing both fluorescent channels. Note how, in general, fluorescence between mother and daughter cells appears to be correlated but, occasionally, a mother cell segregates plasmids unevenly upon division, producing daughter cells with different plasmid configurations (for example the magenta lineage in the kymograph). In the extreme scenario, HT inherits only plasmid of one type to the daughter cell, producing R12 or G1 cells with a probability that can be estimated from a binomial distribution.

In summary, we have established that, as generally assumed by theoretical models of plasmid dynamics (Ilhan et al., 2019; Rodriguez-Beltran et al., 2018; Santer and Uecker, 2019; San Millan et al., 2014) segregation and replication of multicopy plasmids are noise-driven stochastic processes. Now we would like to evaluate if plasmid frequencies are under selection at the level of single cells. To precisely control the concentration of antibiotics inside the microfluidic chip, we developed an automated pressure control system (Ferry et al., 2011) that allows us to introduce different antibiotics into the device and quantify changes in intracellular plasmid frequency in response to environmental change. So we introduced HT cells into the device and observed them for 15 h previous to the introduction to the antibiotic following a ramp protocol: linearly increasing the concentration of antibiotic until reaching a lethal dose and maintaining that concentration constant until all cells are dead.

When introducing ampicillin, we found that the distribution of Δ relative intensity remained symmetric with respect to zero, implying that AMP is not selecting for pBGT-1 plasmids at the level of individual cells. We repeated this microfluidic experiment, now introducing CAZ to select for pBRT-12 plasmids, and confirmed that the shape of the resulting distribution of Δ relative intensity was not skewed towards DsRed. Fig. 3G illustrates violin plots of Δ relative intensity for different selective pressures. Note that, independently of the environmental condition, the shape of the distributions is qualitatively the same (for AMP a Normal distribution with $\mu = -0.00073$, $\sigma^2 = 0.0129$, and for CAZ with $\mu = 0.01298$, $\sigma^2 = 0.0098$). We performed a non-parametric Kolmogorov-Smirnov normality test comparing each distribution against a theoretical Normal distribution with the corresponding μ and σ^2 (H_0: the distribution is not Normal, p-values = (0.527, 0.493, 0.8017) for LB, AMP, and CAZ respectively). In conclusion, regardless the selection regime, the distribution of Δ relative intensities follows a Normal distribution, indicating that changes in relative abundances of different plasmids in single-cells are driven by random noise and not by selection.

3.3. Using microchemostats to study plasmid dynamics in bacterial colonies

We have established that selection can modulate plasmid frequency distributions of heterozygous bacterial populations, and also that

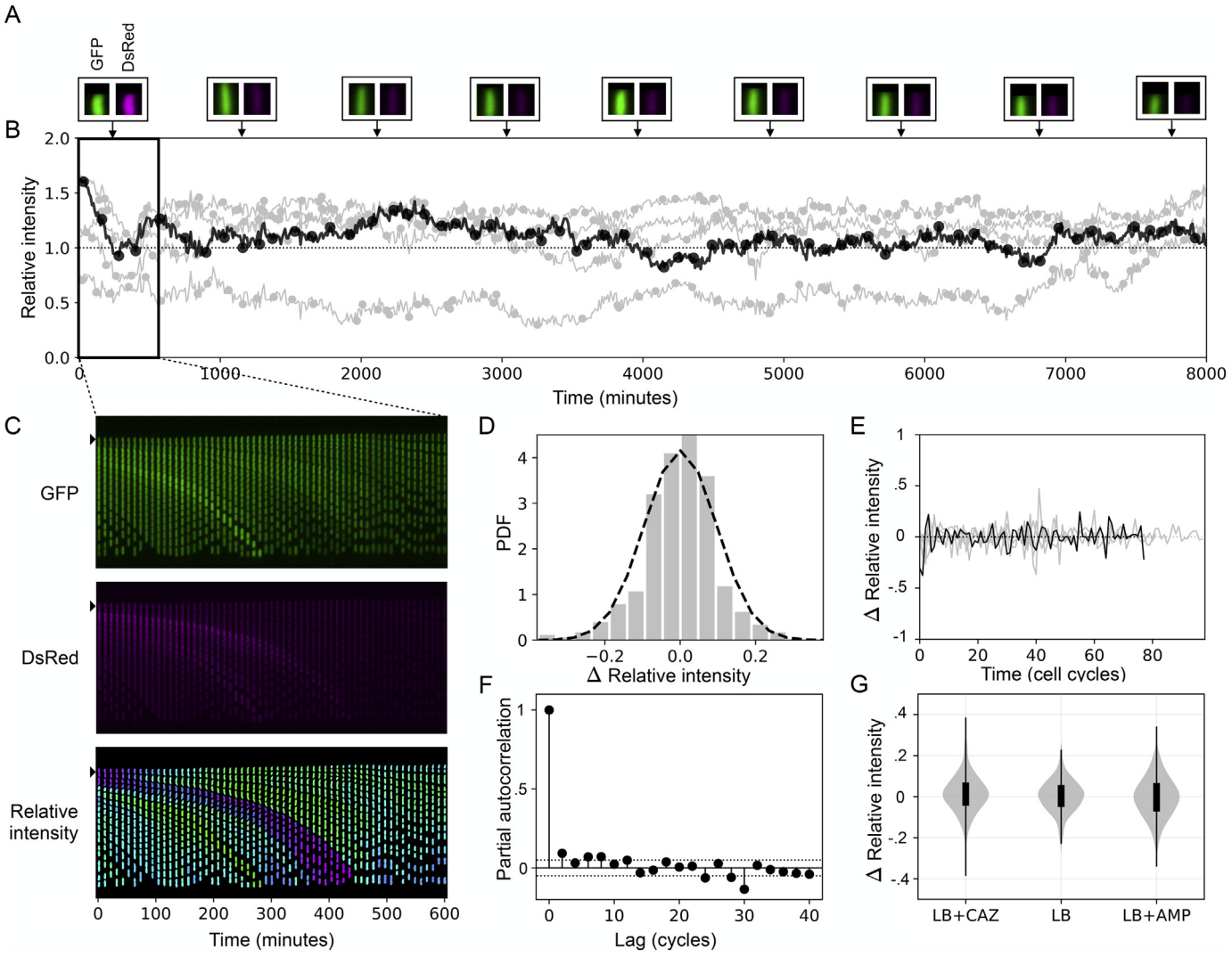

Fig. 3. A) Mother cells at different time-points. Note how the intensity in GFP and DsRed channels changes in time. B) Time-series of relative intensity for individual cells in a long-term experiment. In black data obtained from the mother cell illustrated in A), while 4 other cells are shown in grey. Circles represent division events. C) Kymograph showing the progeny of the mother cell shown in A). From the images obtained in GFP (top) and DsRed (middle), we can use image processing to estimate the relative intensity of each cell (bottom). D) Probability density function of the difference in relative fluorescence of an individual cell between consecutive frames. This distribution can be approximated by a Normal distribution with mean near zero and $\sigma^2 = 0.096$. E) Δ relative intensity as a function of time for cells shown in B). F) Partial autocorrelation function of Δ relative intensity. G) Distributions of Δ relative intensity are normally distributed. A symmetric distribution suggests a random walk that is not correlated with the selective pressure imposed by the environment (left: ceftazidime, middle: drug-free, and right: ampicillin).

intracellular plasmid dynamics is a noise-driven process that does not seem to be affected by selection. Therefore we argue that the shift in fluorescence observed at a population-level must be a consequence of antibiotics selecting for subpopulations with different plasmid configurations. To evaluate this hypothesis and to study the effect on selection in heterozygous populations, we used a different microfluidic device that provides high-throughput time-resolved information about thousands of individual cells simultaneously.

Microchemostats are designed to cultivate bacterial colonies for long periods of time in controlled and well-mixed environments (Mondragón-Palomino et al., 2011; Moffitt et al., 2012; Lopatkin et al., 2016; Li et al., 2019). In particular, here we use a microchemostat adapted from (Mondragón-Palomino et al., 2011) that consists of two parts: the signal generator and the cell confinement region. In the confinement section there are 48 rectangular chambers distributed in four rows. Each containment chamber measures $40 \times 50 \times 0.95\ \mu m^3$, with two sides open to a large channel where media is introduced and cells are washed out of the device. Since *E. coli* cells are approximately 1 μm in diameter, confining them in these microfluidic traps allows the simultaneous observation of a colony of approximately 500 cells in the same focal plane. Furthermore, as with the dual-input mother machine, we can use a signal generator to dynamically control the extracellular concentration of antibiotics.

3.3.1. *Heteroplasmy is unstable in environments with constant selection*

Fig. 4 illustrates an experiment where a population of HT cells was cultured in drug-free media for 6 h, followed by the introduction of antibiotics using a linear ramp. When drug concentration reached a lethal dose (4 *mg/ml* for AMP and 8 *μg/ml* for CAZ), the concentration of antibiotics was maintained constant until all cells were dead (see Supplementary Movies S2 and S3). Fig. 4C shows montages of selected traps at different time-points (CAZ in the top and AMP at the bottom).

We used our image processing pipeline to analyze all traps containing cells growing exponentially after growing overnight inside the device. As in the flow cytometry data, we measured the relative and absolute intensity of each individual cell but, as opposed to flow cytometry data, our microchemostat allows us to track cells in time and perform lineage reconstruction. In particular, we obtained 557 lineages,

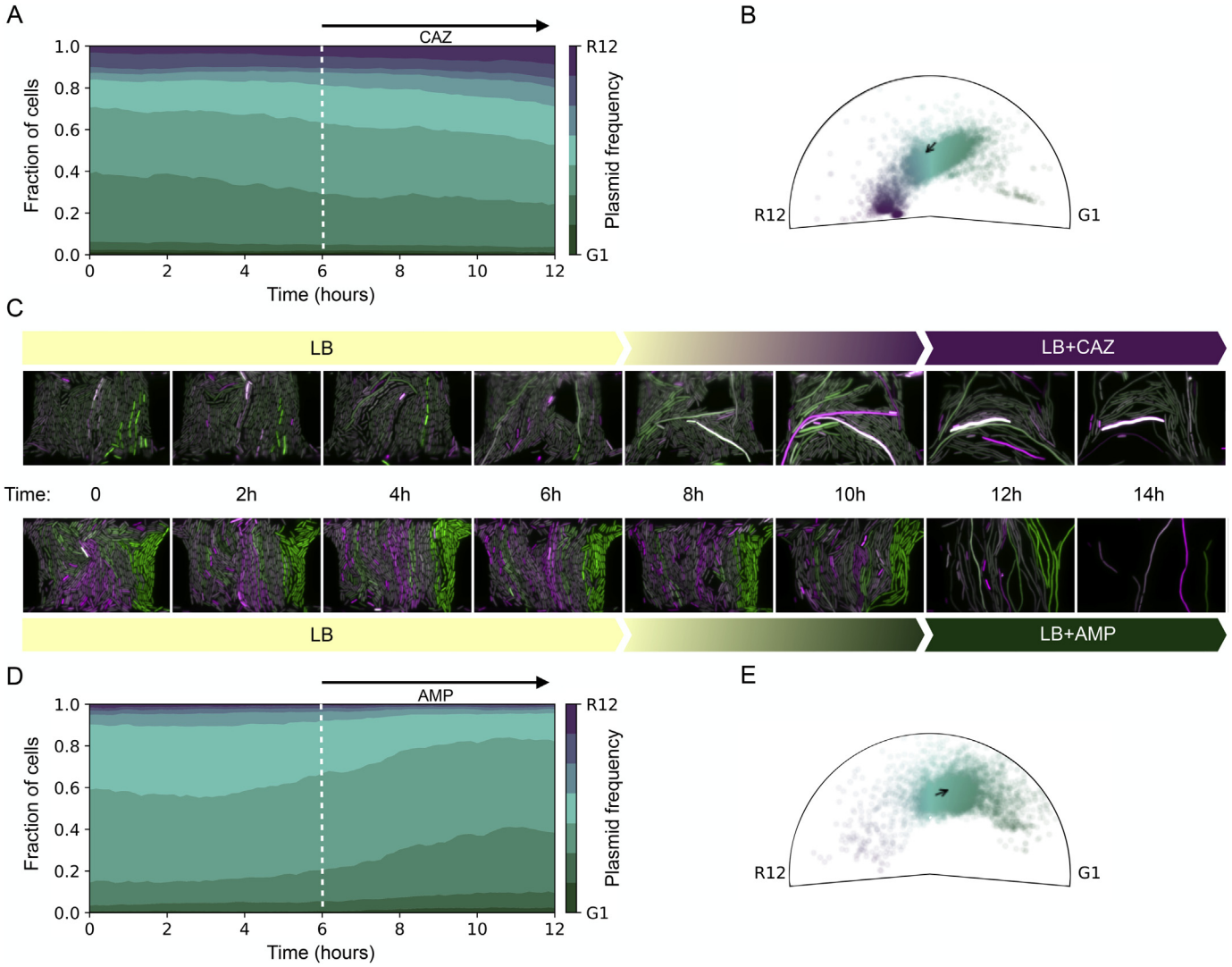

Fig. 4. A) Plasmid fraction as a function of time for a population of HT cells exposed to a ramp of CAZ. B) Polar distribution of cells at the end of the experiment. The black arrow represents changes in the mean plasmid frequency of the population, before and after antibiotic exposure. C) Montage of microscopy images (GFP channel in green, and DsRed in magenta, with both channels overlaid). D) Fraction of cells with a higher proportion of pBGT-1 plasmids is increased when AMP is introduced into the device. *E*-F) Population-level distribution at the end of the experiment. Note how the black arrow points towards higher values of GFP, suggesting that the mean plasmid frequency of the population moved towards cells carrying relatively more copies of pBGT-1. (For interpretation of the references to colour in this figure legend, the reader is referred to the web version of this article.)

corresponding to 5,870 cells in the CAZ experiment and 498 lineages of 5,754 cells for AMP. Of course, as the colony is growing exponentially, most cells are pushed out of the trap and washed out of the device, so only a few lineages were observed from start to end of the experiment. We recovered 48 complete lineages for CAZ and 46 for AMP and, consistent with the results shown in Fig. 3G, the resulting time-series were not correlated with the selective pressure imposed by the environment.

Now, by clustering the population according to their relative fluorescent intensity, we determined the fraction of cells with different plasmid frequencies. As illustrated in Fig. 4A, exposing a population of HT cells to CAZ produces an increase in the fraction of cells with high levels of DsRed and low intensity values of GFP, implying that selection favours cells with a higher proportion of pBRT-12 plasmids. The black arrow in the polar distributions shown in Fig. 4B denotes changes in the mean relative intensity of the population after 6 h of exposure to CAZ and, as expected, points towards R12. In contrast, when introducing AMP into the device, the fluorescent intensity distribution appeared to be shifted towards GFP, consequence of G1 cells being positively selected for, a feature that can be seen in Fig. 4D and in the polar distribution shown in Fig. 4E.

Notably, the shift is larger when using CAZ than in the presence of AMP. This is explained by $bla_{\mathrm{TEM-1}}$ providing partial resistance to AMP and therefore the relative fitness (and thus the rate of fixation) is larger for R12 in ceftazidime than G1 in ampicillin. In any case, HT cells reduced in frequency and are destined to be outcompeted by homozygous subpopulations: R12 if using CAZ or G1 in an AMP environment. This is consistent with previous studies showing that heteroplasmy is unstable in constant environmental conditions (Rodriguez-Beltran et al., 2018). It has also been reported that fluctuating environments can stably maintain intracellular genetic diversity for long-time intervals, so in the following section we will evaluate this hypothesis using microchemostats.

3.3.2. *Fluctuating environments stabilize genetic diversity*

By alternating both antibiotics periodically, we experimentally explored if fluctuating environmental conditions can stabilize plasmid-mediated heterozygosis. Specifically, we introduced HT cells into the device and observed them in LB for about 3 h before introducing antibiotics. To implement a fluctuating selection regime, we generated a

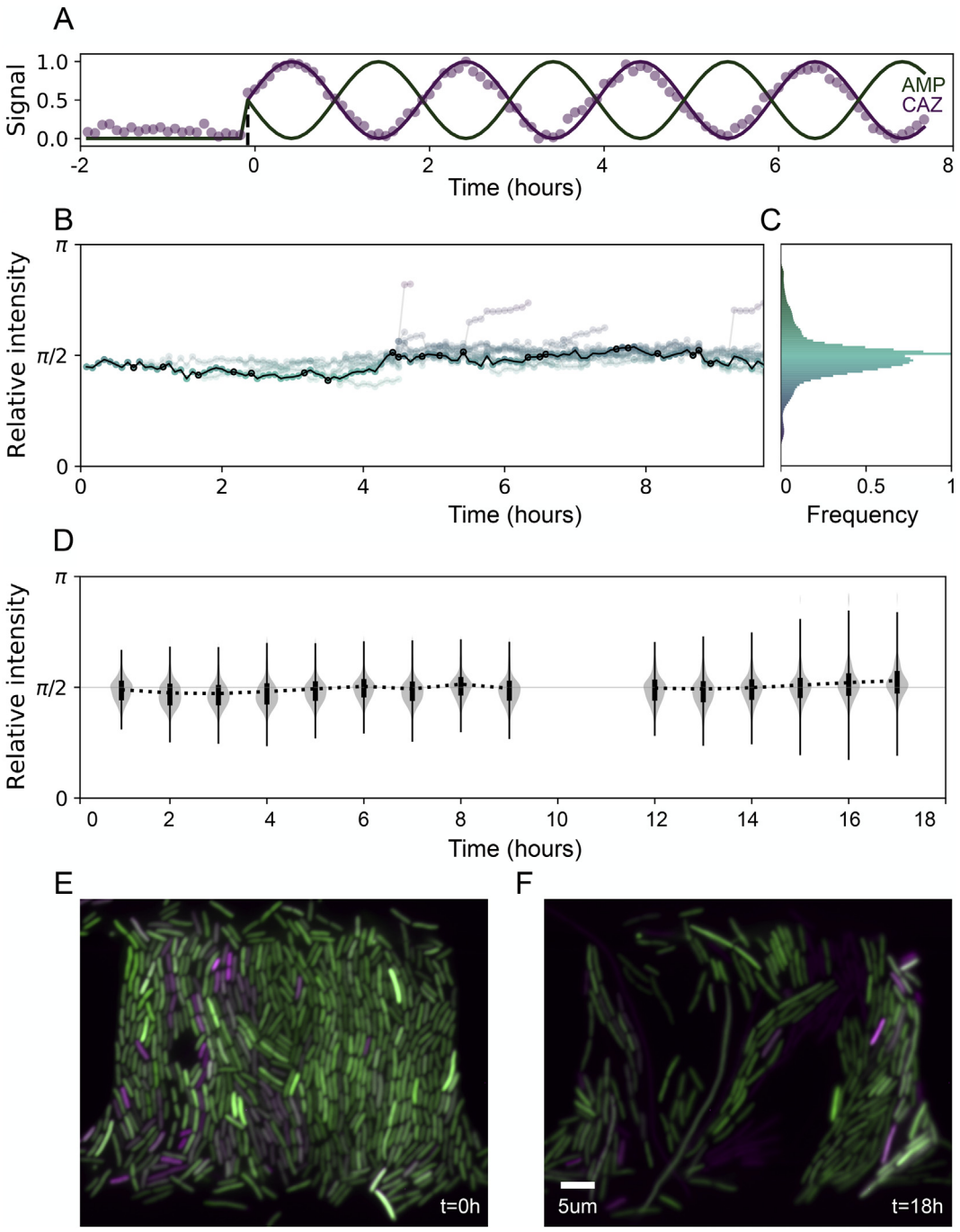

Fig. 5. A) Oscillatory drug deployment protocol consisting on CAZ (magenta) and AMP (green) being alternated every two hours. Magenta circles correspond to measured values of fluorescent dye also introduced into the device together with CAZ. B) Black line represents a single-cell lineage obtained from a time-lapse movie of a microchemostat. Black circles represent division events and relative fluorescence of daughter cells is illustrated in cyan. C) Relative fluorescent distribution obtained after 18 h of exposure to fluctuating CAZ and AMP selective pressures. D) Population-level relative intensity distributions at different time-points. A consequence of alternating selection for both alleles is that intermediate values of relative fluorescence are maintained for long time periods, suggesting that genetic diversity can be stabilized in fluctuating environmental conditions. E) Microscopy images at the beginning (left) and at the end (right) of the experiment. Note how, after 18 h of fluctuating selection, the resulting population is composed of R12 and G1 cells, but also of HT cells. (For interpretation of the references to colour in this figure legend, the reader is referred to the web version of this article.)

sinusoidal signal of period 2 h such that, when CAZ concentration is at 100%, then AMP is at 0%, and vice versa, as illustrated in Fig. 5C (in green the concentration of AMP and in magenta of CAZ, both normalized to the same critical concentrations used before). We diluted a fluorescent dye to one of the antibiotic inputs to calibrate the height of the syringes, but this also allowed us to use the fluorescent microscope to validate that cells are exposed to the expected proportion between both antibiotics. Magenta dots represent DsRed measurements in a cell-free area of the device and correspond very precisely with the drug-deployment protocol sent by the signal generator.

Fig. 5B shows a lineage reconstruction where the black line corresponds to an individual cell observed for the complete duration of the experiment, while other cells in the lineage are illustrated in cyan. Note how, as previously shown in the mother-machine, the intracellular plasmid dynamics appears to be random and is not correlated with the environmental signal. A consequence of the random segregation and

replication of plasmids is that, after only a few generations, the distribution of alleles in the population presents a large variance, as shown in Fig. 5C.

As we have previously argued, we cannot make inferences about the stability of plasmid-mediated heterozygosis from single-cell data. So we included the remaining cells to our analysis and estimated relative intensity distributions at different time-points. Fig. 5D shows violin plots representing the distribution estimated every hour. As opposed to the constant drug environment discussed previously, in the alternating selection regime, the mean relative intensity is centered around HT throughout the duration of the experiment (although the variance increases in time). Fig. 5E and F show composite images at $t = 0$ and at $t = 18$ h, extracted from Supplementary Movie S4, revealing the presence of G1 and R12 cells at the end of the experiment and, crucially, of cells still bearing both plasmids.

4. Discussion

The rate at which pathogenic bacteria evolve resistance to antibiotics is dramatically decreasing the efficacy of current antimicrobial treatments. It may seem a surprising statement but, after more than a century of using antimicrobials in the clinic, some of the evolutionary forces that drive the emergence and spread of drug resistance in pathogenic bacteria are still poorly understood. For instance, most of our understanding of drug resistance adaptation assumes that clonal populations growing in constant environments present similar susceptibility and resistance profiles to antibiotics, while actually clinical isolates can present a high degree of heterorresistance generated, in many cases, by heterogeneous expression of plasmid-borne resistance genes (Andersson et al., 2019).

In a previous paper (Rodriguez-Beltran et al., 2018), we used mathematical modelling and experimental evolution to argue that multi-copy plasmids can provide a platform to increase intracellular genetic diversity and, in consequence, enhance the probability of survival to dynamic environmental conditions. Here we used microfluidics and fluorescence microscopy to study, with single-cell resolution, the effect of selection in the relative abundance of incompatible plasmids carrying different versions of an antibiotic resistance gene and a fluorescent marker. As expected, in the absence of selection, the stochastic nature of plasmid replication and segregation renders plasmids unstable and decreases allele frequency in the population. In contrast, positive selection for plasmid-encoded genes stabilizes plasmids at high copy-numbers, increasing the frequency of the corresponding allele and promoting resistance to the antibiotics used.

Of course, natural environments are not constant but alternate selection between subpopulations with different genetic configurations. Therefore, in dynamic environments, it may be optimal for bacterial populations to present genetic heterogeneity, thus increasing the probability that some individuals are pre-adapted to future environmental conditions (Ackermann, 2015). Indeed, in agreement with previous laboratory studies (Rodriguez-Beltran et al., 2018), we showed that fluctuating selection - in this case, alternating the extracellular concentration of different β-lactam antibiotics - maintained intracellular genetic diversity in the population for longer than constant environmental regimes.

Although previous studies have successfully deployed a combination of experimental evolution (MacLean and San Millan, 2015; Harrison and Brockhurst, 2012; Holloway et al., 2007), genome sequencing (San Millan et al., 2014; Harrison et al., 2015; Porse et al., 2016) and mathematical modeling (Stewart and Levin, 1977; Santer and Uecker, 2019; San Millan et al., 2014; Wein et al., 2019; Yurtsev et al., 2013) to evaluate the population dynamics that emerge in response to different environmental conditions, the intrinsic resolution of flow cytometers and qPCR machines do not allow us to dissect stochastic plasmid dynamics (generated by randomly replicating and partitioning plasmids) from deterministic population-level effects (e.g. differences in relative fitness associated with expressing multiple alleles). So, in this paper, we used single-cell microfluidics to generate high-throughput fluorescent intensity data of heterozygous bacterial populations exposed to a range of selective regimes.

In particular, we used computer vision algorithms to analyze time-lapse movies acquired in multiple fluorescence channels, allowing us to characterize the allele distribution in the population in terms of the relative and absolute fluorescent intensities of its constituent cells. This allowed us to evaluate directly the contribution of selection and random genetic drift in the rate of fixation and extinction of different plasmid variants. We showed, using a mother-machine to restrain individual cells and follow them for very long periods, that changes in plasmid frequency are the consequence of a noise-driven process that is not correlated with the direction and strength of selection imposed by the environment.

We conclude by arguing that imaging and microfluidics can provide a potentially useful approach to study the interaction between intracellular plasmid dynamics and selection imposed by the environment, and therefore could be used to increase our understanding of the complex interaction between mobile genetic elements, their bacterial hosts, and the environment.

Supplementary data to this article can be found online at https://doi.org/10.1016/j.plasmid.2020.102517.

Acknowledgements

We are grateful to Craig MacLean, Octavio Mondragón-Palomino, David Zamorano and members of the Fuentes-Hernández and Peña-Miller groups for helpful discussions, comments, and suggestions. Also to Jose Escudero for generous gifts of strains and plasmids. We are also thankful with Andrés Saralegui Amaro from Laboratorio Nacional de Microscopía Avanzada for assistance using the flow cytometer. JCRHB is a doctoral student in Programa de Doctorado en Ciencias Biomédicas, Universidad Nacional Autónoma de México, and received fellowship 59691 from CONACYT. This work was supported by a Newton Advanced Fellowship awarded by the Royal Society (NA140196) and by CONACYT (Ciencia Básica grant A1-S-32164), both awarded to RPM. AFH and RPM were also supported by PAPIIT-UNAM (grants IA201418 and IN209419, respectively). ASM is supported by a Miguel Servet Fellowship (MS15-00012). JRB is a recipient of a Juan de la Cierva-Incorporación Fellowship (IJC2018-035146-I).

References

Ackermann, M., 2015. A functional perspective on phenotypic heterogeneity in microorganisms. Nat. Rev. Microbiol. 13 (8), 497–508.
Ackermann, M., Stearns, S.C., Jenal, U., 2003. Senescence in a bacterium with asymmetric division. Science 300, 1920.
Alekshun, M.N., Levy, S.B., 2007. Molecular mechanisms of antibacterial multidrug resistance. Cell 128, 1037–1050.
Andersson, D.I., Nicoloff, H., Hjort, K., 2019. Mechanisms and clinical relevance of bacterial heteroresistance. Nat. Rev. Microbiol. 1.
Arnoldini, M., et al., 2014. Bistable expression of virulence genes in salmonella leads to the formation of an antibiotic-tolerant subpopulation. PLoS Biol. **12**.
Aroonnual, A., Janvilisri, T., Ounjai, P., Chankhamhaengdecha, S., 2017. Microfluidics: innovative approaches for rapid diagnosis of antibiotic-resistant bacteria. Essays Biochem. 61, 91–101.
Artemova, T., Gerardin, Y., Dudley, C., Vega, N.M., Gore, J., 2015. Isolated cell behavior drives the evolution of antibiotic resistance. Mol. Syst. Biol. 11.
Babić, A., Lindner, A.B., Vulić, M., Stewart, E.J., Radman, M., 2008. Direct visualization of horizontal gene transfer. Science 319, 1533–1536.
Bahl, M.I., Rensen, S., Hestbjerg Hansen, L., 2004. Quantification of plasmid loss in escherichia coli cells by use of flow cytometry. FEMS Microbiol. Lett. 232, 45–49.
Balleza, E., Kim, J.M., Cluzel, P., 2018. Systematic characterization of maturation time of fluorescent proteins in living cells. Nat. Methods 15, 47.
Balomenos, A.D., et al., 2017. Image analysis driven single-cell analytics for systems microbiology. BMC Syst. Biol. 11, 43.
Baltekin, Ö., Boucharin, A., Tano, E., Andersson, D.I., Elf, J., 2017. Antibiotic susceptibility testing in less than 30 min using direct single-cell imaging. Proc. Natl. Acad. Sci. 114, 9170–9175.
Band, V.I., Weiss, D.S., 2019. Heteroresistance: A cause of unexplained antibiotic treatment failure? PLoS Pathog. 15.

Bañuelos-Vazquez, L.A., et al., 2019. Conjugative transfer between rhizobium etli endosymbionts inside the root nodule. Environ. Microbiol. 21, 3430–3441.
Barlow, M., Hall, B.G., 2002. Predicting evolutionary potential: in vitro evolution accurately reproduces natural evolution of the tem β-lactamase. Genetics 160, 823–832.
Barlow, M., Hall, B.G., 2003. Experimental prediction of the natural evolution of antibiotic resistance. Genetics 163, 1237–1241.
Baumgart, L., Mather, W., Hasty, J., 2017. Synchronized dna cycling across a bacterial population. Nat. Genet. 49, 1282–1285.
Baxter, J.C., Funnell, B.E., 2015. Plasmid partition mechanisms. Plasmids: Biology and Impact in Biotechnology and Discovery 133–155.
Bennett, M.R., Hasty, J., 2009. Microfluidic devices for measuring gene network dynamics in single cells. Nat. Rev. Genet. 10, 628–638.
Berg, S., et al., 2019a. ilastik: interactive machine learning for (bio)image analysis. Nat. Methods 16, 1226–1232.
Berg, S., et al., 2019b. ilastik: Interactive machine learning for (bio) image analysis. Nat. Methods 1–7.
Bergmiller, T., et al., 2017. Biased partitioning of the multidrug efflux pump acrab-tolc underlies long-lived phenotypic heterogeneity. Science 356, 311–315.
Boedicker, J.Q., Vincent, M.E., Ismagilov, R.F., 2009. Microfluidic confinement of single cells of bacteria in small volumes initiates high-density behavior of quorum sensing and growth and reveals its variability. Angew. Chem. Int. Ed. 48, 5908–5911.
Boucher, H.W., et al., 2009. Bad bugs, no drugs: no eskape! An update from the infectious diseases society of america. Clin. Infect. Dis. 48, 1–12.
del Campo, I., et al., 2012. Determination of conjugation rates on solid surfaces. Plasmid 67, 174–182.
Chait, R., Ruess, J., Bergmiller, T., Tkačik, G., Guet, C.C., 2017. Shaping bacterial population behavior through computer-interfaced control of individual cells. Nat. Commun. 8, 1–11.
Connell, J.L., Kim, J., Shear, J.B., Bard, A.J., Whiteley, M., 2014. Real-time monitoring of quorum sensing in 3d-printed bacterial aggregates using scanning electrochemical microscopy. Proc. Natl. Acad. Sci. 111, 18255–18260.
Del Solar, G., Espinosa, M., 2000. Plasmid copy number control: an ever-growing story. Mol. Microbiol. 37, 492–500.
El Meouche, I., Dunlop, M.J., 2018. Heterogeneity in efflux pump expression predisposes antibiotic-resistant cells to mutation. Science 362, 686–690.
Ferry, M.S., Razinkov, I.A., Hasty, J., 2011. Microfluidics for synthetic biology: from design to execution. In: Methods in enzymology. 497. Elsevier, pp. 295–372.
Galitski, T., et al., 1995. Evidence that f plasmid transfer replication underlies apparent adaptive mutation. Science 268, 421–423.
Ghozzi, S., Ng, J.W., Chatenay, D., Robert, J., 2010. Inference of plasmid-copy-number mean and noise from single-cell gene expression data. Phys. Rev. E 82, 051916.
Hall, J.P., Wright, R.C., Guymer, D., Harrison, E., Brockhurst, M.A., 2020. Extremely fast amelioration of plasmid fitness costs by multiple functionally diverse pathways. Microbiology 166, 56–62.
Harrison, E., Brockhurst, M.A., 2012. Plasmid-mediated horizontal gene transfer is a coevolutionary process. Trends Microbiol. 20, 262–267.
Harrison, E., Guymer, D., Spiers, A.J., Paterson, S., Brockhurst, M.A., 2015. Parallel compensatory evolution stabilizes plasmids across the parasitism-mutualism continuum. Curr. Biol. 25, 2034–2039.
Holloway, A.K., Palzkill, T., Bull, J.J., 2007. Experimental evolution of gene duplicates in a bacterial plasmid model. J. Mol. Evol. 64, 215–222.
Hsu, T.-M., Chang, Y.-R., 2019. High-copy-number plasmid segregationâ€ single-molecule dynamics in single cells. Biophys. J. 116, 772–780.
Ilhan, J., et al., 2019. Segregational drift and the interplay between plasmid copy number and evolvability. Mol. Biol. Evol. 36, 472–486.
Ishii, K., Hashimoto-Gotoh, T., Matsubara, K., 1978. Random replication and random assortment model for plasmid incompatibility in bacteria. Plasmid 1, 435–445.
Kaiser, M., et al., 2018. Monitoring single-cell gene regulation under dynamically controllable conditions with integrated microfluidics and software. Nat. Commun. 9, 1–16.
Kamentsky, L., et al., 2011. Improved structure, function and compatibility for cellprofiler: modular high-throughput image analysis software. Bioinformatics 27, 1179–1180.
Keasling, J., Palsson, B., 1989. Cole1 plasmid replication: a simple kinetic description from a structured model. J. Theor. Biol. 141, 447–461.
Knox, J.R., 1995. Extended-spectrum and inhibitor-resistant tem-type beta-lactamases: mutations, specificity, and three-dimensional structure. Antimicrob. Agents Chemother. 39, 2593.
Łapińska, U., Glover, G., Capilla-Lasheras, P., Young, A.J., Pagliara, S., 2019. Bacterial ageing in the absence of external stressors. Philos. Trans. R. Soc. B 374, 20180442.
Le Roux, F., Binesse, J., Saulnier, D., Mazel, D., 2007. Construction of a vibrio splendidus mutant lacking the metalloprotease gene vsm by use of a novel counterselectable suicide vector. Appl. Environ. Microbiol. 73, 777–784.
Li, B., Qiu, Y., Song, Y., Lin, H., Yin, H., 2019. Dissecting horizontal and vertical gene transfer of antibiotic resistance plasmid in bacterial community using microfluidics. Environ. Int. 131, 105007.
Lindner, A.B., Madden, R., Demarez, A., Stewart, E.J., Taddei, F., 2008. Asymmetric segregation of protein aggregates is associated with cellular aging and rejuvenation. Proc. Natl. Acad. Sci. 105, 3076–3081.
Løbner-Olesen, A., 1999. Distribution of minichromosomes in individual escherichia coli cells: implications for replication control. EMBO J. 18, 1712–1721.
Locke, J.C., Elowitz, M.B., 2009. Using movies to analyse gene circuit dynamics in single cells. Nat. Rev. Microbiol. 7, 383–392.
Loftie-Eaton, W., et al., 2016. Evolutionary paths that expand plasmid host-range: implications for spread of antibiotic resistance. Mol. Biol. Evol. 33, 885–897.
Long, Z., et al., 2013. Microfluidic chemostat for measuring single cell dynamics in bacteria. Lab Chip 13, 947–954.
Lopatkin, A.J., et al., 2016. Antibiotics as a selective driver for conjugation dynamics. Nat. Microbiol. 1, 1–8.
Lopatkin, A.J., et al., 2017. Persistence and reversal of plasmid-mediated antibiotic resistance. Nat. Commun. 8, 1–10.
Lugagne, J.-B., Lin, H., Dunlop, M.J., 2019. Delta: Automated cell segmentation, tracking, and lineage reconstruction using deep learning. bioRxiv 720615.
MacLean, R.C., San Millan, A., 2015. Microbial evolution: towards resolving the plasmid paradox. Curr. Biol. 25, R764–R767.
Mathis, R., Ackermann, M., 2016. Response of single bacterial cells to stress gives rise to complex history dependence at the population level. Proc. Natl. Acad. Sci. 113, 4224–4229.
Mochizuki, A., Yahara, K., Kobayashi, I., Iwasa, Y., 2006. Genetic addiction: selfish gene's strategy for symbiosis in the genome. Genetics 172, 1309–1323.
Moffitt, J.R., Lee, J.B., Cluzel, P., 2012. The single-cell chemostat: an agarose-based, microfluidic device for high-throughput, single-cell studies of bacteria and bacterial communities. Lab Chip 12, 1487–1494.
Mondragón-Palomino, O., Danino, T., Selimkhanov, J., Tsimring, L., Hasty, J., 2011. Entrainment of a population of synthetic genetic oscillators. Science 333, 1315–1319.
Mosheiff, N., et al., 2017. Correlations of single-cell division times with and without periodic forcing. arXiv preprint arXiv:1710.00349.
Mroczkowska, J.E., Barlow, M., 2008. Fitness trade-offs in blatem evolution. Antimicrob. Agents Chemother. 52, 2340–2345.
Münch, K., Münch, R., Biedendieck, R., Jahn, D., Müller, J., 2019. Evolutionary model for the unequal segregation of high copy plasmids. PLoS Comput. Biol. 15, e1006724.
Ng, J.W., Chatenay, D., Robert, J., Poirier, M.G., 2010. Plasmid copy number noise in monoclonal populations of bacteria. Phys. Rev. E 81, 011909.
Nicoloff, H., Hjort, K., Levin, B.R., Andersson, D.I., 2019. The high prevalence of antibiotic heteroresistance in pathogenic bacteria is mainly caused by gene amplification. Nat. Microbiol. 4, 504–514.
Nordström, K., 1984. Equipartition and other modes of partition: on the interpretation of curing kinetics using rep (ts) plasmids. Mol. Gen. Genet. MGG 198, 185–186.
Nordström, K., Molin, S., Light, J., 1984. Control of replication of bacterial plasmids: genetics, molecular biology, and physiology of the plasmid r1 system. Plasmid 12, 71–90.
Novick, R.P., 1987. Plasmid incompatibility. Microbiol. Rev. 51, 381.
Pan, L., et al., 2011. Maskless plasmonic lithography at 22 nm resolution. Sci. Rep. 1, 175.
Patange, O., et al., 2018. Escherichia coli can survive stress by noisy growth modulation. Nat. Commun. 9, 1–11.
Paulsson, J., 2002. Multileveled selection on plasmid replication. Genetics 161, 1373–1384.
Paulsson, J., Ehrenberg, M., 2001. Noise in a minimal regulatory network: plasmid copy number control. Q. Rev. Biophys. 34, 1–59.
Peña-Miller, R., Rodrguez-González, R., MacLean, R.C., San Millan, A., 2015. Evaluating the effect of horizontal transmission on the stability of plasmids under different selection regimes. Mob. Genet. Elem. 5, 29–33.
Pinilla-Redondo, R., Cyriaque, V., Jacquiod, S., Sørensen, S.J., Riber, L., 2018. Monitoring plasmid-mediated horizontal gene transfer in microbiomes: recent advances and future perspectives. Plasmid 99, 56–67.
Porse, A., Schønning, K., Munck, C., Sommer, M.O., 2016. Survival and evolution of a large multidrug resistance plasmid in new clinical bacterial hosts. Mol. Biol. Evol. 33, 2860–2873.
Potvin-Trottier, L., Luro, S., Paulsson, J., 2018. Microfluidics and single-cell microscopy to study stochastic processes in bacteria. Curr. Opin. Microbiol. 43, 186–192.
Reyes-Lamothe, R., et al., 2013. High-copy bacterial plasmids diffuse in the nucleoid-free space, replicate stochastically and are randomly partitioned at cell division. Nucleic Acids Res. 42, 1042–1051.
Rochman, N., Si, F., Sun, S.X., 2016. To grow is not enough: impact of noise on cell environmental response and fitness. Integr. Biol. 8, 1030–1039.
Rodriguez-Beltran, J., et al., 2018. Multicopy plasmids allow bacteria to escape from fitness trade-offs during evolutionary innovation. Nature Ecol. & Evol. 2, 873.
Rodriguez-Beltran, J., et al., 2019. Genetic dominance governs the evolution and spread of mobile genetic elements in bacteria. bioRxiv 863472.
Sachs, C.C., et al., 2016. Image-based single cell profiling: High-throughput processing of mother machine experiments. PLoS One 11.
Salje, J., 2010. Plasmid segregation: how to survive as an extra piece of dna. Crit. Rev. Biochem. Mol. Biol. 45, 296–317.
Salverda, M.L., De Visser, J.A.G., Barlow, M., 2010. Natural evolution of tem-1 β-lactamase: experimental reconstruction and clinical relevance. FEMS Microbiol. Rev. 34, 1015–1036.
San Millan, A., 2018. Evolution of plasmid-mediated antibiotic resistance in the clinical context. Trends Microbiol. 26, 978–985.
San Millan, A., et al., 2014. Positive selection and compensatory adaptation interact to stabilize non-transmissible plasmids. Nat. Commun. 5, 5208.
San Millan, A., Escudero, J.A., Gifford, D.R., Mazel, D., MacLean, R.C., 2016. Multicopy plasmids potentiate the evolution of antibiotic resistance in bacteria. Nat. Ecol. & Evol. 1, 1–8.
Santer, M., Uecker, H., 2019. Evolutionary rescue and drug resistance on multicopy plasmids. bioRxiv.
Santos-Lopez, A., et al., 2017. A naturally occurring single nucleotide polymorphism in a multicopy plasmid produces a reversible increase in antibiotic resistance. Antimicrob. Agents Chemother. 61 e01735–16.
Schneider, C.A., Rasband, W.S., Eliceiri, K.W., 2012. Nih image to imagej: 25 years of image analysis. Nat. Methods 9, 671–675.
Seneta, E., Tavaré, S., 1983. Some stochastic models for plasmid copy number. Theor. Popul. Biol. 23, 241–256.

Shintani, M., et al., 2014. Single-cell analyses revealed transfer ranges of incp-1, incp-7, and incp-9 plasmids in a soil bacterial community. Appl. Environ. Microbiol. 80, 138–145.
Stewart, F.M., Levin, B.R., 1977. The population biology of bacterial plasmids: a priori conditions for the existence of conjugationally transmitted factors. Genetics 87, 209–228.
Summers, D.K., 1991. The kinetics of plasmid loss. Trends Biotechnol. 9, 273–278.
Sun, L., et al., 2018. Effective polyploidy causes phenotypic delay and influences bacterial evolvability. PLoS Biol. 16, e2004644.
Taheri-Araghi, S., Jun, S., 2015. Single-cell cultivation in microfluidic devices. In: Hydrocarbon and Lipid Microbiology Protocols. Springer, pp. 5–16.
Tal, S., Paulsson, J., 2012. Evaluating quantitative methods for measuring plasmid copy numbers in single cells. Plasmid 67, 167–173.
Tomanek, I., et al., 2020. Gene amplification as a form of population-level gene expression regulation. Nat. Ecol. & Evol. 1–14.
Van Valen, D.A., et al., 2016. Deep learning automates the quantitative analysis of individual cells in live-cell imaging experiments. PLoS Comput. Biol. 12.
Wallden, M., Fange, D., Lundius, E.G., Baltekin, Ö., Elf, J., 2016. The synchronization of replication and division cycles in individual e. coli cells. Cell 166, 729–739.
Wang, X., et al., 2014. Heteroresistance at the single-cell level: adapting to antibiotic stress through a population-based strategy and growth-controlled interphenotypic coordination. MBio 5 e00942–13.
Wang, Y., Penkul, P., Milstein, J.N., 2016. Quantitative localization microscopy reveals a novel organization of a high-copy number plasmid. Biophys. J. 111, 467–479.
Wein, T., Hülter, N.F., Mizrahi, I., Dagan, T., 2019. Emergence of plasmid stability under non-selective conditions maintains antibiotic resistance. Nat. Commun. 10.
Wiedenbeck, J., Cohan, F.M., 2011. Origins of bacterial diversity through horizontal genetic transfer and adaptation to new ecological niches. FEMS Microbiol. Rev. 35, 957–976.
Young, J.W., et al., 2012. Measuring single-cell gene expression dynamics in bacteria using fluorescence time-lapse microscopy. Nat. Protoc. 7, 80.
Yurtsev, E.A., Chao, H.X., Datta, M.S., Artemova, T., Gore, J., 2013. Bacterial cheating drives the population dynamics of cooperative antibiotic resistance plasmids. Mol. Syst. Biol. 9.
Zhang, L., et al., 2012. Inkjet printing high-resolution, large-area graphene patterns by coffee-ring lithography. Adv. Mater. 24, 436–440.